The Senescence-Associated-Secretory Phenotype constituting HIF-1α activation is independent of micronuclei induction and associated cGAS-mediated interferon response

Deng Lin[1,8], Celestine Ho[2,3,8], Remigio Picone[4,5,8], Fieda Abderazzaq[6], Nicole Flanagan[6], Boon Chuan Low[2,7], Selwin K. Wu[4,5]*

[1] Institute of Molecular Physiology, Shenzhen Bay Laboratory, Shenzhen, China

[2]Mechanobiology Institute, National University of Singapore, Singapore

[3]Department of Biomedical Engineering, National University of Singapore, Singapore

[4]Department of Cell Biology, Harvard Medical School, Boston, MA, USA

[5]Department of Pediatric Oncology, Dana-Farber Cancer Institute, Boston, MA, USA

[6]Center for Cancer Computational Biology, Department of Biostatistics and Computational Biology, Dana-Farber Cancer Institute, Boston, MA, USA

[7]Department of Biological Sciences and NUS College, National University of Singapore, Singapore

[8]Equal contributions

* Correspondence: selwin_wu@mail.dfci.harvard.edu, Present address: Mechanobiology Institute, National University of Singapore, Singapore

ABSTRACT

The Senescence-Associated Secretory Phenotype (SASP), characterized by the upregulation of inflammatory cytokines, is triggered during senescence by anti-proliferation stresses, such as replicative exhaustion and centrosome amplification. Previously, we have discovered that centrosome amplification activates a non-canonical SASP that is dominated by HIF-1α-induced inflammatory cytokines instead of the NFκb activation in canonical SASP. HIF-1α is not only activated in centrosome amplification, oncogene, and gamma-irradiation-induced senescence[1] but also induced in replicative exhaustion-induced senescence. Another major consequence of centrosome amplification is micronuclei generation from chromosome missegregation. The micronuclei could have triggered SASP by activating cGAS/Sting innate immune response[2]. However, it has been shown that micronuclei from chromosome missegregation fail to activate cGAS/Sting-mediated innate immune response[3-5]. Indeed, here we further demonstrate that moderate chromosome missegregation by centrosome amplification or mitotic kinase monopolar

spindle 1 inhibition, which is known to generate micronuclei, fails to induce senescence and cGAS-mediated interferon response. In summary, we provide evidence that the Senescence-Associated-Secretory Phenotype constitutes hypoxia-inducible factor-alpha activation, independent of chromosome missegregation triggering cGAS-mediated innate immune interferon response.

INTRODUCTION

Cellular senescence is characterized by the upregulation of pro-inflammatory cytokines, a phenomenon termed the Senescence-Associated-Secretory Phenotype (SASP)[6] . Cellular senescence is triggered by many stresses[7] , including replicative exhaustion[8] and centrosome amplification[1]. Here, we will focus on centrosome amplification and replicative exhaustion-induced senescence. Centrosomes are microtubule organizing centers, which in turn support cellular processes such as cell division and adhesion[9]. In most normal cells, centrosomes are duplicated once during each cell division such that G1 phase cells typically have one centrosome and mitotic cells have two. By contrast, senescent and cancer cells commonly exhibit increased numbers of centrosomes, termed centrosome amplification. Notably, centrosome amplification can induce proliferation arrest by PIDDosome multiprotein complex[10] and Hippo pathway-mediated mechanisms. Centrosome amplification also stimulates reactive oxygen species production[1] to upregulate the expression of SASP factors. Of note, these secreted SASP factors induce cell-cell contact disruption[11], tumor growth[12], and invasion[1].

During cell division, centrosome amplification promotes chromosome missegregation that generates micronuclei[13]. Micronuclei generated in centrosome amplification cells could have triggered SASP, by activating cGAS/Sting[14]. Cytosolic DNA sensor cyclic guanosine monophosphate (GMP)-AMP synthase (cGAS) functions as a cytosolic DNA sensor that activates the innate immune interferon response when bound to dsDNA in the cytosol[15]. In brief, activated cGAS, when bound to dsDNA, converts ATP and guanosine triphosphate (GTP) to 2′3′-cyclic GMP-AMP (cGAMP). cGAMP binds and activates stimulator of interferon genes (STING). Thus, resulting in TANK-binding kinase 1 kinase-dependent phosphorylation, nuclear translocation of interferon regulatory factor 3, and transcriptional activation of interferon-

stimulated genes[16]. Thus, missegregated chromosomes forming micronuclei with defective nuclear envelope, that are exposed to the cytoplasm, have been reported to activate cGAS/Sting[2].

However, recent reports indicate that micronuclei from chromosome missegregation fail to activate cGAS/Sting mediated innate immune response[3-5]. cGAS localization to nuclear envelope-ruptured micronuclei during interphase was reported to be rare[3-5], with cGAS more often binding to micronuclei during mitosis and remaining on cytosolic chromatin. Notably, cGAS accumulation during mitosis did not activate STING or trigger the interferon response in the subsequent interphase[3, 5]. Amongst the cellular senescence triggers, gamma-irradiation activated STING independently of micronuclei formation and cGAS localization to micronuclei, suggesting that micronuclei are not the trigger for cGAS/STING pathway activation[5]. Indeed, STING-mediated interferon response after irradiation is linked to cytosolic mitochondria DNA release instead[3]. The presence of histones in micronuclei was found to be a potential inhibitory factor, preventing cGAS activation[5]. Consistent with reports that micronuclei do not activate cGAS, here we demonstrate that moderate chromosome missegregation induction by mitotic kinase monopolar spindle 1 (MPS1) inhibition or centrosome amplification, which generates micronuclei[5, 13] fails to induce senescence and interferon response.

Besides the implications of micronuclei and cGAS/Sting signaling in senescence, we have discovered that hypoxia signaling is activated in centrosome amplification, oncogene, and gamma-irradiation-induced senescence[1]. HIF are key transcription factors that regulate oxygen sensing and mediate the hypoxic response[17]. Activation of HIF triggers the transcription of genes crucially involved in cancer[18] and immunity[19], including cytokines such as IL8, IL6, ANGPTL4, VEGF, and PDGF, which are commonly observed in SASP [6, 20-22].

Cellular senescence triggers such as constitutively active Ras overexpression, which promotes invasion, metastasis, and cell extrusion[23, 24 25], also activate HIF-1α[1, 26, 27]. Similarly, gamma-irradiation, which promotes inflammation and senescence, triggers HIF activation[1, 28]. Besides centrosome amplification, oncogene, and gamma-irradiation-induced senescence, we here find that senescence is induced by replicative exhaustion. Replicative exhaustion-induced senescence is often partly a result of telomeric dysfunction (telomere uncapping) resulting from repeated cell

division[29]. Although evidence suggests that hypoxia and HIF activation can prevent or delay cells from entering senescence[30]. Nevertheless, the HIF activity of cells once they have entered replicative exhaustion-induced senescence remains unknown. Here, applying Gene Set Enrichment Analysis (GSEA)[31] on whole-transcriptome datasets, we reveal hypoxia induction and response in replicative exhausted senescent cells but not in quiescence cells.

In summary, we demonstrate that the Senescence-Associated-Secretory Phenotype induced by centrosome amplification and replicative exhaustion constitutes hypoxia-inducible factor-alpha pathway activation, independent of chromosome missegregation triggering the cGAS-mediated inteferon response.

MATERIALS & METHODS

Cell culture

All source cell culture was maintained in media containing plasmocin (1:5000 dilution, Invivogen) to prevent mycoplasma contamination. Culture plates were briefly coated with 40μg/ml of fibronectin (Sigma) and glass coverslips were incubated in 40 μg/ml fibronectin for at least 2 hours. Human mammary epithelial MCF10A cells were maintained at 37^0C with 5% CO2 atmosphere and cultured as previously described[14]. In brief, MCF10A cells were cultured in phenol red-free DMEM/F12 (Invitrogen) supplemented with 5% horse serum (Sigma), 20ng/ml epidermal growth factor (EGF; Sigma), 10mg/ml insulin (Invitrogen), 100 mg/ml hydrocortisone (Sigma), 1ng/ml cholera toxin (Sigma) and 100 IU/ml penicillin and 100 μg/ml streptomycin (Invitrogen). WI38 lung fibroblast cells, obtained from the ATCC, were cultured in ATCC-formulated Eagle's Minimum Essential Medium containing 10% FBS.

To conditionally overexpress PLK4, lentiviral vectors pLenti-CMV-TetR-Blast (17492, Addgene) and pLenti-CMV/TO-Neo-Dest (17292, Addgene) were used. Wild-type PLK4 and PLK4 1–608 cDNAs (control 608) were cloned using the Gateway system into the pLenti-CMV/TO-Neo-Dest vector. W138 lung fibroblasts were coinfected with a lentivirus containing the TetR and with the lentivirus containing the wild-type PLK4 or control 608 open reading frames.

Induction of centrosome amplification and senescence

At day 0, control 608 and PLK4 cells were gently dissociated into single cells, then seeded at low density into media with 2μg/ml of doxycycline such that they were ~80% confluent on day 5. After ~48 hours of doxycycline incubation, the culture media with doxycycline was replaced. On day 5, cells are gently dissociated into single cells before reseeding into 6 well plates to ~80% confluent on day 7. Because control 608 cells grow faster than PLK4 induced cells, control 608 cells are seeded at ~2.5 times lower density than PLK4 induced cells. Cells at ~80% confluency are analysed either at day 7 or day 8. Media is left unchanged for ~3 days before analysis.

Generation of tetraploids and 'evolved' tetraploids with normal centrosome numbers

To generate G1 arrested tetraploids, 15cm dishes were seeded with 6 million exponentially growing RPE1-FUCCI cells, such that they were ∼65% confluent the following day. Day 2: 4 μM Dihydrocytochalasin B (DCB) was added to each 15 cm dish for 16 hr. Day 3: DCB-treated cells were washed 5 times for 5 minutes, incubated in medium containing 2.5 μg/ml Hoechst dye for 1 hr, then trypsinized in 0.05% trypsin. G1 diploids (2C DNA content; mCherry+, GFP−) and G1 tetraploids (4C DNA content; mCherry+, GFP−) were isolated by FACS sorting. FACS-sorted cells were seeded on 6 well plates coated with 40μg/ml fibronectin.

Evolved tetraploid RPE-1 cells, kindly provided by Huadi Zhang, with the normal number of centrosomes were derived as described[13]. Briefly, tetraploid RPE-1 cells were treated for 16 hr with 0.2 μm cytochalasin D, and FACS-sorted by DNA content using Hoechst staining (Molecular Probes). The peak of cells with a DNA content of 8C were isolated and cultured for ∼1 week before a second iteration of the FACS sorting to re-isolate 8C cells. A total of 5 purifying cell sortings for ∼6 weeks were required to generate a pure population of proliferating tetraploid cells with normal centrosome numbers.

CRISPR Knockouts and Lentiviral Transduction

The previously described[32] HIF-1α pLenti-CRISPRv2 was a gift from William G. Kaelin, Jr. (Dana-Farber Cancer Institute, Boston, USA). The sgRNA sequence targeting HIF-1α is as follow: '5'- CACCGTGTGAGTTCGCATCTTGATA -'3'. Clonal selection for single-cell clones

after puromycin selection were used for the experiments.

For lentivirus production, 6μg lentiviral constructs, 3 μg psPAX2 (Addgene), and 3 μg pMD2.G (Addgene) were transfected into 293T cells at 80% confluency in a 10-cm dish with 8 ml of media. 20 μl of lipofectamine 3000 (Life Technologies) was used and transfection was performed according to manufacturer's instructions. Virus was harvested at 48 hours and 72 hours post-infection and filtered with a 0.2μm filter[33, 34]. MCF10A cells were infected for 12 hours, with virus containing the genes of interest in the presence of 10 μg/ml polybrene, washed thoroughly, and allowed to recover for 24 hours before any selection.

Antibodies and drugs

Primary antibodies used in this study were: rabbit monoclonal antibodies against cGAS (1:1000 for western blotting; Cell Signaling Technologies catalog number 15102S, clone number D1D3G), mouse monoclonal antibodies against HIF-1α (1:50-1:100 for immunofluorescence; Abcam catalog number ab16066)

Doxycycline (Sigma Aldrich catalog number D3072) was used at 2 mg/ml. TNFα (Roche Diagnostics catalog number 11371843001) was used at 20ng/ml for 2 hours. The following doses of inhibitors were used: 0.1 and 0.2 μM Reversine (Cayman Chemical) 4μM of dihydro cytochalasin B (DCB; Sigma).

Immunofluorescence and live-cell microscopy

Cells were fixed at 4°C with 4% paraformaldehyde in cytoskeleton stabilization buffer (10mM PIPES at pH 6.8, 100mM KCl, 300mM sucrose, 2mM EGTA, and 2mM MgCl2) on ice for 25 min and subsequently permeabilized with 0.2% Triton-X in PBS for 10 minutes at room temperature[33, 35-40]. Fixed cells were blocked with 5% BSA in TBS overnight at 4°C. Primary antibodies were incubated overnight at 4°C for HIF-1α and 45 minutes at room temperature for p65/RELA. For all immunostaining, secondary Alexa Fluor antibodies were incubated at room temperature for an hour.

For live cell imaging, time-lapse images were collected with a Nikon Ti inverted microscope with 20x wide-field optics equipped with a perfect focus system, a Hamamatsu ORCA ER

cooled CCD camera controlled with Nikon NIS-Element software, and an OkoLab 37°C, 5% CO_2 microscope chamber.

Media Swap Motility Assay Cells were plated at 0.5-1x10^6 per well in 6 well plates and allowed to attach for 24h. Then, cells were starved in serum free medium for two hours and incubated in 0.5% horse serum media for another 12 hours. Conditioned medium from cells with or without centrosome amplification were collected and centrifuged at 5000 rpm for 20 minutes to eliminate any detached cells or debris. Conditioned medium was then added to cells and the effect of the swapped conditioned medium on the cellular motility was imaged with bright field microscopy (Nikon Ti).

NextSeq500 RNA Library Preparation and Sequencing

RNA quantity was determined on the Qubit using the Qubit RNA Assay Kit (Life Tech) and RNA quality was determined on the Bioanalyzer using the RNA Pico Kit (Agilent). Using the NEB Next Ultra RNA Library Prep Kit for Illumina (NEB), which selects for poly(A) mRNA, 100ng of total RNA was used for cDNA library construction, according to the manufacturer's protocol. Following library construction, DNA quantity was determined using the Qubit High Sensitivity DNA Kit (Life Technologies), and library insert size was determined using the Bioanalyzer High Sensitivity Chip Kit (Agilent). Finally, qPCR was performed using the Universal Library Quantification Kit for Illumina (Kapa Biosystems) and run on the 7900HT Fast qPCR machine (ABI) for quantification and normalization of libraries. Libraries that passed quality control were diluted to 2nM DNA content using sterile water and then sequenced on the NextSeq500 (Illumina) at a final concentration of 12pM, according to the manufacturer's instructions.

RNA Sequencing Analysis

Sequencing reads were aligned to the reference genome using the RNA-specific STAR aligner using default parameters[41]. The quality of sequencing runs and alignments was assessed by RNA-SeQC[42]. The featureCounts tool was used to count sequencing reads mapped to the reference genome at the gene level[43]. The counts were subsequently normalized between samples using DESeq2 to control for experimental variation[44]. Differential expression analysis was performed between the desired experimental contrasts using DESeq2.

Gene Set Enrichment Analysis

We used GSEA v3.0 to examine the association between gene sets and gene expression. Normalised read counts from DESeq2 analysis were used for GSEA. Genes with a 0 read count in either control or experimental group were excluded. GSEA was performed using gene sets as permutation type, 1,000 permutations and log2 ratio of classes as metric for ranking genes. To construct a HIF-α signature upregulated gene set, we performed RNA sequencing of MCF10A cells after overnight treatment with 1μm of DMOG, with DMSO-treated cells as control. We included genes that were upregulated by DMOG in both DESeq and DESeq2 analysis (p(adjusted)<0.05, fold change $\geq$ 4, Supplementary Table 1). To construct a DNA-damage senescence gene set we performed RNA sequencing of MCF10A cells 7 days after exposure to 12Gy of γ-irradiation. We obtained published data sets to construct both upregulated and downregulated core senescence gene sets[45].

Quantitative RT-PCR Total RNA was isolated using the RNAeasy Mini Kit (Qiagen), and cDNA was synthesised using SuperScript III (Invitrogen) according to manufacturer instructions. Quantitative RT-qPCR was performed in triplicate using SYBR Green (Life Technologies) on a ViiA 7 Real-Time PCR machine (Thermo Fisher Scientific) with GAPDH as an internal normalisation control. Sequences of qPCR primers for cGAS are as follows: Forward primer: 5'-gggagccctgctgtaacacttcttat-3', Reverse primer: 5'-cctttgcatgcttgggtacaaggt-3'

RESULTS AND DISCUSSION

The hallmark hypoxia genes are induced in cellular senescence

The transcriptome datasets used here were validated by analysis of their senescence expression pattern. Many senescence-associated markers result from altered transcription, but the senescent phenotype is variable. This variability might be due to tissue and cell-type differences, differences in the senescence trigger[46] , and the dynamic nature of gene expression in senescent cells[47-49]. Despite variabilities in the senescent phenotype, a core transcriptome signature of a list of upregulated and downregulated genes has recently been identified as a useful marker to

consistently identify senescent cells[45]. Thus, we employ this universal senescent gene set to confirm the senescent identity of cells that underwent gamma-irradiation, replicative exhaustion and constitutive Ras oncogene-induced senescence. MCF10A cells were exposed to 12 Gy of gamma-irradiation, whereas the replicative exhaustion and constitutive active Ras-induced IMR90 cells transcriptome were obtained from published datasets[50] investigating the senescence-associated secretory phenotype. Seven days post-irradiation, the transcriptomes of control cells and gamma-irradiated cells were compared. GSEA determines the transcriptional program activated by identifying coordinated changes in a defined set of gene expressions[31]. Gene set enrichment analysis revealed a strong association between gamma-irradiation (Figure 1a, b), replicative exhaustion (Figure 1c,d), and constitutive-active Ras oncogene (Figure 1e, f) induced genes with both upregulated and downregulated senescence gene sets.

We then used GSEA to identify transcriptional signatures that are commonly activated in gamma-irradiation, replicative exhaustion, and constitutive-active Ras oncogene-induced senescence. We employ the hallmark gene sets from the Molecular Signatures Database (MSigDB)[31, 51, 52]. Hallmark gene sets summarize and represent specific, well-defined biological states or processes and display coherent expression. These gene sets were generated by a computational methodology based on identifying gene set overlaps and retaining genes that display coordinate expression, thus reducing data noise and redundancy. Strikingly, the hypoxia hallmark was identified as a common expression signature profile from our GSEA of replicative exhausted, gamma-irradiated, and Ras-induced cells (Figure 1g,h). The hallmark hypoxia signature was ranked 3rd and 8th in replicative and Ras-induced senescence, respectively. The hallmark hypoxia signature was ranked 17th in our irradiated cells, ahead of the p53 hallmark response- which is a key feature of cellular senescence. Commonly induced hallmark gene sets also include the inflammatory response, NFκB activation, and IL2/STAT5 signaling (Figure 1h). These immune-associated expression programs were known to be commonly induced in cellular senescence[53]. The top 30 genes in the hallmark hypoxia GSEA leading-edge subset from gamma-irradiated, replicative exhausted and constitutive active Ras-induced includes well-validated HIF-1α targets such as ANGPTL4, PDGFB and VEGFA (Fig 1i, j, k).

HIF-1α target genes are induced in SASP and replicative exhaustion-induced senescence but not in cellular quiescence

HIF-1α is a critical sensor of low oxygen levels[54, 55]. In normoxia, prolyl hydroxylases (PHDs) hydroxylate HIF-1α, triggering von Hippel–Lindau-mediated ubiquitination and proteasomal degradation[OBJ]. Conversely, hypoxia inhibits PHDs and stabilizes HIF-1α, which then translocate into the nucleus and dimerizes with constitutively expressed HIF-1β, activating the HIF complex and triggering the transcription of genes promoting inflammation and cancer[56].

A gene-expression signature of HIF-α activation is derived from transcriptomic analysis of MCF10A normal breast epithelial cells treated with Dimethyloxalylglycine, N-(Methoxyoxoacetyl)-glycine methyl ester (DMOG)[1]. DMOG promotes the steady-state accumulation of HIF-1α because it inhibits the EGLN/PHD prolyl hydroxylases, which mark HIF-1α for proteasomal degradation[57]. Strikingly, expression of SASP factors in general is induced in DMOG-treated cells (Figure 2a,b). Common SASP factors such as IGFBP3, IL8, and VEGF are among the top 20 genes in the SASP GSEA leading-edge subset (Figure 2b). This custom HIF-1α activation gene set is significantly enriched in replicative exhaustion-induced senescent cells (Fig 2c,d). By contrast, our analysis of two previously published datasets for the induction of cellular quiescence in IMR90 fibroblasts[58] (Figure 2e,f) and LFS MDAH041 fibroblast cells[8] (Figure 2g,h) revealed that both the hallmark hypoxia and HIF-1α activation gene sets were either not induced (Figure 3e,f) or significantly suppressed (Figure 2g,h). Thus, suggesting that the induction of HIF-1α genes is specific to the induction of cellular senescence but not quiescence.

Centrosome amplification induces paracrine MCF10A cell protrusions and senescence in WI38 fibroblasts

Next, we analyze the consequence of centrosome amplification-induced senescence. Centrosome amplification was induced in cells by overexpressing Polo-like kinase 4 (PLK4), the master regulatory kinase for centrosome duplication[59, 60]. PLK4 was transiently induced, and subsequent analysis was performed at time points where increased PLK4 mRNA expression was no longer

detectable[61]. In most experiments described below, cells with the transient overexpression of a truncated PLK4 mutant (Control 608) with kinase activity, which did not localize to the centrosomes[62], were used as the negative control.

We previously found that centrosome amplification can induce paracrine invasion by activating a SASP[1]. The induction of paracrine motility by secreted factors is a hallmark of SASP[6]. To visualize whether cells with centrosome amplification can induce dynamic protrusions of normal cells in a paracrine manner, we swapped the conditioned medium between MCF10A cells with centrosome amplification and the conditioned medium from control cells without centrosome amplification. As expected, the control conditioned medium did not alter the protrusion velocity of cells with centrosome amplification (Fig.3a,b,d and Supplementary Video 1). By contrast, conditioned media from cells with centrosome amplification induced an approximately 2-fold increase in the velocity of leading edge movement in cells lacking centrosome amplification (Fig.3a,c,d and Supplementary Video 2).

Besides Retinal Pigment Epithelial-1 (RPE-1) and MCF-10A epithelial cells entering senescence when induced with extra centrosomes seven days post-induction[1], WI38 lung fibroblasts also exhibit senescence-associated beta-galactosidase activity (~60% positive cells, Fig. 3e,f) when induced with extra centrosomes by transient PLK4 expression. Additionally, senescence-associated heterochromatin foci were observed after the induction of centrosome amplification by transient PLK4 expression in WI38 cells(Fig. 3g,h). As senescence-associated heterochromatin foci is a cell-type specific phenotype[63], senescence-associated heterochromatin foci are not observed in MCF10A or RPE-1 cells (data not shown).

Centrosome amplification induced a non-canonical SASP with an inflammatory response dominated by HIF-1α instead of the classical NFκB

Although centrosome amplification generated many cellular features and gene expression characteristics of senescence, several aspects of the response were distinct from senescence induced by canonical triggers[1]. First, the SASP induced by centrosome amplification was distinct from the SASP induced by conventional triggers dominated by NF-κB activation. NF-κB is generally thought to be the primary determinant of the SASP secretome[64], and DNA damage

signaling was recently shown to activate NF-κB through the transcription factor GATA4[64, 65]. However, centrosome amplification induction of proinflammatory cytokines was modest by comparison with the SASP induced by γ-irradiation or oncogene activation (Fig 4a)[50, 64]. Moreover, there is no detectable GATA4 mRNA in MCF10A cells, with or without centrosome amplification (Fig 4a).

However, by GSEA, we did observe enrichment for NF-κB-regulated genes in the samples where centrosome amplification was induced by PLK4 transient overexpression (Fig 4b). But this enrichment for NF-κB-regulated genes was abolished by CRISPR-mediated gene disruption of HIF-1α (Fig 4c), suggesting that the shared gene targets of HIF-1α with NF-κB is contributing to the enrichment of NF-κB-regulated genes [19]. Additionally, we did not observe a significant enrichment for NF-κB-regulated genes in the samples where centrosome amplification was induced by cytokinesis failure (Fig 4b). Strikingly, quantitative imaging indicated that centrosome amplification in WI38 lung fibroblasts did not result in any detectable increase in the nuclear localization of NF-κB (Fig. 4d,e). Thus, centrosome amplification induces a non-canonical SASP that is dominated by HIF-1α activation.

Centrosome amplification can induce SASP independent of moderate chromosome missegregation and micronuclei activation of cGAS

Second, the effects of centrosome amplification are distinct from those of aneuploidy. Although aneuploidy can induce cell cycle arrest and senescence, it is established that this occurs at high levels of aneuploidy that disrupt DNA replication and cause DNA damage[66, 67]. Accordingly, we confirm that a low level of aneuploidy (MPS1 inhibition by reversine), a comparable level to that induced by centrosome amplification[61], does not trigger proliferation arrest (Fig 5a,b) or induce HIF-1α (Fig 5c,d).

Lastly, senescence from various conventional triggers, for example, 12 Gy gamma-irradiation of MCF10A (Fig 5e,f), triggers an interferon response, possibly due to cytosolic mitochondria DNA release activating STING[3]. However, in the SASP that occurs after centrosome amplification, interferon response genes are suppressed, not induced (Fig 5g,h). A major consequence of centrosome amplification is chromosome missegregation generation of micronuclei. Our data is

consistent with reports indicating that cGAS-mediated interferon response is not activated by micronuclei[3-5]. Moreover, RPE-1 cells, which manifest an upregulation of secreted protein expression after senescence induction by various triggers[66], including centrosome amplification[1], lack detectable expression of cGAS (Fig 5i,j). Thus, indicating that cGAS is not essential for cellular senescence in RPE-1 cells. In conclusion, we provide evidence that the Senescence-Associated-Secretory Phenotype constituting HIF-1α activation is independent of chromosome missegregation triggering the cGAS-mediated innate immune interferon response.

FIGURES

Figure 1. The hallmark hypoxia genes are induced in cellular senescence.

(a,b,c,d,e,f) GSEA shows that the senescence up-regulated (a,c,e) and down-regulated (b,d,f) gene sets are induced in the 12 Gy γ-irradiation (a,b), replicative exhaustion (c,d), and RasG12V-induced cells (e,f).

(g) GSEA shows that the hallmark hypoxia gene set is induced in replicative exhaustion-induced senescence.

(h) Eight hallmark expression signatures are commonly upregulated in 12 Gy γ-irradiation, replicative exhausted, and Ras G12V-induced senescent cells. Venn diagram for the indicated comparisons showing the overlap of the hallmark expression signatures from all experimental conditions. The bottom panel is a table of the hallmark expression signatures with at least an FDR of $q < 0.05$ shared between Ras & replicative-exhaustion, Ras & irradiation, and replicative-exhaustion & irradiation-induced senescence, respectively.

(i,j,k) Heatmaps showing the leading-edge enrichment of the top hallmark hypoxia 30 genes in (i) 12 Gy γ-irradiation, (j) replicative exhaustion, and (k) RasG12V-induced cells.

Figure 2. Activation of HIF target genes triggers SASP factors expression, and replicative exhaustion activates HIF target genes but not in quiescent cells.

(a) GSEA showing that the SASP factors gene set is enriched in DMOG-treated cells.

(b) Heatmap showing the leading-edge enrichment of the top 20 SASP factors in DMOG-treated MCF10A cells.

(c) GSEA showing that the custom HIF-α signature up is enriched in replicative exhausted cells.

(d) Heatmap showing the leading-edge enrichment of the top custom HIF-α signature upregulated 30 genes in replicative exhausted cells.

(e,f,g,h) GSEA showing that the (e,g) hallmark hypoxia and (f,h) custom HIF-α signature up gene sets are suppressed in (e,f) IMR90[58] and (g,h) LFS MDAH041 fibroblast cells[8] undergoing quiescence.

Figure 3. Centrosome amplification induces senescence in WI-38 fibroblast and paracrine cell protrusions.

(a-d) Conditioned media from MCF10A cells with centrosome amplification stimulates the leading-edge displacement of wild-type cells. (a) Representative images of leading-edge displacement in cells with and without centrosome amplification, with or without conditioned media swap. Colour code on the heatmap and images represents the position of leading edge at different time points.

(b,c) Quantitative analysis of leading-edge displacement in MCF10A cells with (PLK4, b) or without (control, c) centrosome amplification, before and after exchange with the indicated conditioned medium.

(d) Conditioned media from MCF10A cells with centrosome amplification significantly increases the average protrusion velocity of control cells. Shown is the average velocity of leading-edge displacement in cells with and without centrosome amplification, with or without conditioned media swap.

(e,f) Increased SA-β-Gal staining in WI38 fibroblasts with centrosome amplification. Representative images (e) and quantification (f) of SA-β-Gal (blue) staining of WI38 fibroblasts with and without centrosome amplification or positive control with doxorubicin treatment.
(g,h) Centrosome amplification induces Senescence-Associated Heterochromatin Foci formation in WI38 cells. Images (g) and quantification (h) of senescence-associated heterochromatin foci (Hoechst) in WI38 cells with and without centrosome amplification.

Figure 4. Centrosome amplification induces a HIF-1α inflammatory response independent of NFκB.

(a) Only modest induction of pro-inflammatory cytokines and undetectable levels of GATA4 or IL6 in MCF10A cells after induction of centrosome amplification. Indicated are the mRNA fold changes of the PLK4 samples relative to the 608 control from RNAseq (left) and RT-qPCR of IL6 (right) in MCF10A cells. Data are means + s.e.m. from n=3 independent experiments, ns, not significant, ****P <0:0001; adjusted P value(grey) analyzed with DESeq2 Wald test.

(b) Induction of NF-κB regulated genes after centrosome amplification from PLK4 transient overexpression, but not from cytokinesis failure. Shown are GSEA FDR: q values and normalized enrichment score(NES) for the indicated cell lines.

(c) CRISPR-mediated gene disruption of HIF1A abolishes the induction of NF-κB regulated genes by centrosome amplification. GSEA revealed a statistically insignificant suppression of NF-κB regulated- genes in sgHIF1A cells with centrosome amplification relative to sgHIF1A control cells.

(d,e) Lack of NF-κB nuclear accumulation after centrosome amplification. (d) Representative images of p65 RELA (NF-κB) and DAPI (grey) in WI38 cells with and without centrosome amplification as compared with TNFα treated cells. (e) Quantification of p65 RELA (NF-κB) nuclear/cytoplasmic ratio in WI-38 cells with or without centrosome amplification as compared to TNFα treatment.

All data are means + s.e.m. from n=3 independent experiments, **P < 0.01, ***P < 0.001,****P <0.0001; analysed with Student's t-test. Scale bars, 50 μm.

Figure 5. Centrosome amplification can induce a SASP independent of chromosome mis-segregation induced inflammatory response.

(a,b) Low-dose MPS inhibition by reversine, at concentrations that generate comparable or higher levels of aneuploidy than centrosome amplification from transient PLK4[61], does not induce proliferation arrest. Representative images (a) and quantification (b) of EdU (red) and DAPI (blue) in MCF10A cells with (PLK4) and without (608) centrosome amplification or control cells treated with 0.1 μm or 0.2μm reversine for 24 hours.

(c,d) Low-dose MPS inhibition by reversine, at concentrations that generate comparable or higher levels of aneuploidy than centrosome amplification from transient PLK4[61], does not induce nuclear HIF-1α. Representative images (c) and quantification (d) of nuclear HIF-1α levels in MCF10A cells with (PLK4) and without (608) centrosome amplification or wild-type cells treated with either 0.1μm or 0.2μm reversine.

(e,f) Induction of interferon-alpha (e) and interferon-gamma (f) response genes in cells after gamma-irradiation by GSEA.
(g,h) Suppression of interferon-alpha and interferon-gamma response expression in cells with centrosome amplification. GSEA revealed the downregulation of genes annotated as Hallmark interferon alpha response (c) and Hallmark interferon-gamma response (d) in MCF10A cells with centrosome amplification relative to control.

(i) Undetectable levels of cGAS in RPE-1 cells. Relative mRNA level of cGAS in BJ, MCF10A and RPE-1 cells by RT-qPCR.

(j) cGAS protein is undetectable in RPE-1 cell lysates. cGAS and GAPDH (loading control) immunoblots of lysates from BJ and RPE-1 cells.

Supplementary Video 1. Conditioned media from control cells does not affect the leading edge movement of cells with centrosome amplification.
Live imaging of MCF10A cells with centrosome amplification before (left) or after (right) control conditioned media swap.

Supplementary Video 2. Conditioned media from MCF10A cells with centrosome amplification stimulates the leading edge movement of control cells. Live imaging of control MCF10A cells without centrosome amplification before (left) or after (right) centrosome amplification conditioned media swap.

Conflict of Interest

The authors declare that the research was conducted without any commercial or financial relationships that could be construed as a potential conflict of interest.

Acknowledgements

We dedicate this work posthumously to J.Campisis for her founding contribution to SASP, which was discovered in her laboratory. We gratefully thank D.Pellman, I. Ghobrial, S. Papathanasiou, A. Spektor, A.J. Holland, W. Johnson, Y. Kaplan, A. Yap, S. Liu, K. Briggs and W. Kaelin for their unstinting support and advice during this project. A.Spektor for gamma irradiation experiments, L. Hodgson and H. Zhang for technical advice and reagents, Y. Wang, D. Deconti, and B. Lawney from the Centre for Cancer Computational Biology and X. Qiu and H. Long from Center for Functional Cancer Epigenetics for help with bioinformatic analysis. SKW was supported by a Leukemia and Lymphoma Society Fellow Award (5454-17) and a Young Individual Research Grant (MOH-OFYIRG20nov-0019) by the National Medical Research Council of Singapore. LD was supported by the National Key Research and Development Program of China (2022YFA1302800) and the National Natural Science Foundation of China (32270779). RP was supported by a Susan G. Komen Postdoctoral Fellowship (PDF15333560). We acknowledge the Nikon Imaging Center at Harvard Medical School for imaging support.

REFERENCES

1. Wu, S.K., Ariffin, J., Tay, S.C. & Picone, R. The variant senescence-associated secretory phenotype induced by centrosome amplification constitutes a pathway that activates hypoxia-inducible factor-1alpha. *Aging Cell* **22**, e13766 (2023).
2. Mackenzie, K.J. *et al.* cGAS surveillance of micronuclei links genome instability to innate immunity. *Nature* **548**, 461-465 (2017).

3. Sato, Y. & Hayashi, M.T. Micronucleus is not a potent inducer of the cGAS/STING pathway. *Life Sci Alliance* **7** (2024).
4. Flynn, P.J., Koch, P.D. & Mitchison, T.J. Chromatin bridges, not micronuclei, activate cGAS after drug-induced mitotic errors in human cells. *Proc Natl Acad Sci U S A* **118** (2021).
5. Takaki, T., Millar, R., Hiley, C.T. & Boulton, S.J. Micronuclei induced by radiation, replication stress, or chromosome segregation errors do not activate cGAS-STING. *Mol Cell* **84**, 2203-2213 e2205 (2024).
6. Coppe, J.P., Desprez, P.Y., Krtolica, A. & Campisi, J. The senescence-associated secretory phenotype: the dark side of tumor suppression. *Annu Rev Pathol* **5**, 99-118 (2010).
7. Ben-Porath, I. & Weinberg, R.A. When cells get stressed: an integrative view of cellular senescence. *J Clin Invest* **113**, 8-13 (2004).
8. Purcell, M., Kruger, A. & Tainsky, M.A. Gene expression profiling of replicative and induced senescence. *Cell Cycle* **13**, 3927-3937 (2014).
9. Akhmanova, A., Stehbens, S.J. & Yap, A.S. Touch, grasp, deliver and control: functional cross-talk between microtubules and cell adhesions. *Traffic* **10**, 268-274 (2009).
10. Fava, L.L. *et al.* The PIDDosome activates p53 in response to supernumerary centrosomes. *Genes Dev* **31**, 34-45 (2017).
11. Mangold, S. *et al.* Hepatocyte growth factor acutely perturbs actin filament anchorage at the epithelial zonula adherens. *Curr Biol* **21**, 503-507 (2011).
12. Angelini, P.D. *et al.* Constitutive HER2 signaling promotes breast cancer metastasis through cellular senescence. *Cancer Res* **73**, 450-458 (2013).
13. Ganem, N.J., Godinho, S.A. & Pellman, D. A mechanism linking extra centrosomes to chromosomal instability. *Nature* **460**, 278-282 (2009).
14. Gluck, S. *et al.* Innate immune sensing of cytosolic chromatin fragments through cGAS promotes senescence. *Nat Cell Biol* **19**, 1061-1070 (2017).
15. Li, X. *et al.* Cyclic GMP-AMP synthase is activated by double-stranded DNA-induced oligomerization. *Immunity* **39**, 1019-1031 (2013).
16. Ablasser, A. & Hur, S. Regulation of cGAS- and RLR-mediated immunity to nucleic acids. *Nat Immunol* **21**, 17-29 (2020).
17. Kietzmann, T., Mennerich, D. & Dimova, E.Y. Hypoxia-Inducible Factors (HIFs) and Phosphorylation: Impact on Stability, Localization, and Transactivity. *Front Cell Dev Biol* **4**, 11 (2016).
18. Miroshnikova, Y.A. *et al.* Tissue mechanics promote IDH1-dependent HIF1alpha-tenascin C feedback to regulate glioblastoma aggression. *Nat Cell Biol* **18**, 1336-1345 (2016).
19. Palazon, A., Goldrath, A.W., Nizet, V. & Johnson, R.S. HIF transcription factors, inflammation, and immunity. *Immunity* **41**, 518-528 (2014).
20. Maxwell, P.J. *et al.* HIF-1 and NF-kappaB-mediated upregulation of CXCR1 and CXCR2 expression promotes cell survival in hypoxic prostate cancer cells. *Oncogene* **26**, 7333-7345 (2007).
21. Liu, X., He, L., Stensaas, L., Dinger, B. & Fidone, S. Adaptation to chronic hypoxia involves immune cell invasion and increased expression of inflammatory cytokines in rat carotid body. *Am J Physiol Lung Cell Mol Physiol* **296**, L158-166 (2009).

22. Yoshida, D., Kim, K., Noha, M. & Teramoto, A. Hypoxia inducible factor 1-alpha regulates of platelet derived growth factor-B in human glioblastoma cells. *J Neurooncol* **76**, 13-21 (2006).
23. Wu, S.K., Lagendijk, A.K., Hogan, B.M., Gomez, G.A. & Yap, A.S. Active contractility at E-cadherin junctions and its implications for cell extrusion in cancer. *Cell Cycle* **14**, 315-322 (2015).
24. Wu, S.K. *et al.* Cortical F-actin stabilization generates apical-lateral patterns of junctional contractility that integrate cells into epithelia. *Nat Cell Biol* **16**, 167-178 (2014).
25. Wu, S.K. & Yap, A.S. Patterns in space: coordinating adhesion and actomyosin contractility at E-cadherin junctions. *Cell Commun Adhes* **20**, 201-212 (2013).
26. Mazure, N.M., Chen, E.Y., Yeh, P., Laderoute, K.R. & Giaccia, A.J. Oncogenic transformation and hypoxia synergistically act to modulate vascular endothelial growth factor expression. *Cancer Res* **56**, 3436-3440 (1996).
27. Mazure, N.M., Chen, E.Y., Laderoute, K.R. & Giaccia, A.J. Induction of vascular endothelial growth factor by hypoxia is modulated by a phosphatidylinositol 3-kinase/Akt signaling pathway in Ha-ras-transformed cells through a hypoxia inducible factor-1 transcriptional element. *Blood* **90**, 3322-3331 (1997).
28. Moeller, B.J., Cao, Y., Li, C.Y. & Dewhirst, M.W. Radiation activates HIF-1 to regulate vascular radiosensitivity in tumors: role of reoxygenation, free radicals, and stress granules. *Cancer Cell* **5**, 429-441 (2004).
29. Rossiello, F., Jurk, D., Passos, J.F. & d'Adda di Fagagna, F. Telomere dysfunction in ageing and age-related diseases. *Nat Cell Biol* **24**, 135-147 (2022).
30. Welford, S.M. & Giaccia, A.J. Hypoxia and senescence: the impact of oxygenation on tumor suppression. *Mol Cancer Res* **9**, 538-544 (2011).
31. Subramanian, A. *et al.* Gene set enrichment analysis: a knowledge-based approach for interpreting genome-wide expression profiles. *Proc Natl Acad Sci U S A* **102**, 15545-15550 (2005).
32. Cho, H. *et al.* On-target efficacy of a HIF-2alpha antagonist in preclinical kidney cancer models. *Nature* **539**, 107-111 (2016).
33. Smutny, M. *et al.* Multicomponent analysis of junctional movements regulated by myosin II isoforms at the epithelial zonula adherens. *PLoS One* **6**, e22458 (2011).
34. Moore, T. *et al.* Self-organizing actomyosin patterns on the cell cortex at epithelial cell-cell junctions. *Biophys J* **107**, 2652-2661 (2014).
35. Han, S.P. *et al.* Cortactin scaffolds Arp2/3 and WAVE2 at the epithelial zonula adherens. *J Biol Chem* **289**, 7764-7775 (2014).
36. Leerberg, J.M. *et al.* Tension-sensitive actin assembly supports contractility at the epithelial zonula adherens. *Curr Biol* **24**, 1689-1699 (2014).
37. Gomez, G.A. *et al.* An RPTPalpha/Src family kinase/Rap1 signaling module recruits myosin IIB to support contractile tension at apical E-cadherin junctions. *Mol Biol Cell* **26**, 1249-1262 (2015).
38. Wu, S.K., Budnar, S., Yap, A.S. & Gomez, G.A. Pulsatile contractility of actomyosin networks organizes the cellular cortex at lateral cadherin junctions. *Eur J Cell Biol* **93**, 396-404 (2014).

39. Acharya, B.R. *et al.* Mammalian Diaphanous 1 Mediates a Pathway for E-cadherin to Stabilize Epithelial Barriers through Junctional Contractility. *Cell Rep* **18**, 2854-2867 (2017).
40. Wu, S.K. *et al.* A morphogenic cascade emerges from the co-evolution of spheroid fluidization and fracturing of multicellular barriers. *bioRxiv*, 2023.2009.2025.559247 (2023).
41. Dobin, A. *et al.* STAR: ultrafast universal RNA-seq aligner. *Bioinformatics* **29**, 15-21 (2013).
42. DeLuca, D.S. *et al.* RNA-SeQC: RNA-seq metrics for quality control and process optimization. *Bioinformatics* **28**, 1530-1532 (2012).
43. Liao, Y., Smyth, G.K. & Shi, W. featureCounts: an efficient general purpose program for assigning sequence reads to genomic features. *Bioinformatics* **30**, 923-930 (2014).
44. Anders, S. & Huber, W. Differential expression analysis for sequence count data. *Genome Biol* **11**, R106 (2010).
45. Hernandez-Segura, A. *et al.* Unmasking Transcriptional Heterogeneity in Senescent Cells. *Curr Biol* **27**, 2652-2660 e2654 (2017).
46. Sharpless, N.E. & Sherr, C.J. Forging a signature of in vivo senescence. *Nat Rev Cancer* **15**, 397-408 (2015).
47. Hoare, M. *et al.* NOTCH1 mediates a switch between two distinct secretomes during senescence. *Nat Cell Biol* **18**, 979-992 (2016).
48. Lee, S. & Schmitt, C.A. The dynamic nature of senescence in cancer. *Nat Cell Biol* **21**, 94-101 (2019).
49. Schmitt, C.A. The persistent dynamic secrets of senescence. *Nat Cell Biol* **18**, 913-915 (2016).
50. Acosta, J.C. *et al.* A complex secretory program orchestrated by the inflammasome controls paracrine senescence. *Nat Cell Biol* **15**, 978-990 (2013).
51. Liberzon, A. *et al.* Molecular signatures database (MSigDB) 3.0. *Bioinformatics* **27**, 1739-1740 (2011).
52. Liberzon, A. *et al.* The Molecular Signatures Database (MSigDB) hallmark gene set collection. *Cell Syst* **1**, 417-425 (2015).
53. Lasry, A. & Ben-Neriah, Y. Senescence-associated inflammatory responses: aging and cancer perspectives. *Trends Immunol* **36**, 217-228 (2015).
54. Iommarini, L., Porcelli, A.M., Gasparre, G. & Kurelac, I. Non-Canonical Mechanisms Regulating Hypoxia-Inducible Factor 1 Alpha in Cancer. *Front Oncol* **7**, 286 (2017).
55. Semenza, G.L. Hypoxia-inducible factor 1: master regulator of O2 homeostasis. *Curr Opin Genet Dev* **8**, 588-594 (1998).
56. Ruas, J.L. & Poellinger, L. Hypoxia-dependent activation of HIF into a transcriptional regulator. *Semin Cell Dev Biol* **16**, 514-522 (2005).
57. Laitala, A. & Erler, J.T. Hypoxic Signalling in Tumour Stroma. *Front Oncol* **8**, 189 (2018).
58. Tasdemir, N. *et al.* BRD4 Connects Enhancer Remodeling to Senescence Immune Surveillance. *Cancer Discov* **6**, 612-629 (2016).
59. Bettencourt-Dias, M. *et al.* SAK/PLK4 is required for centriole duplication and flagella development. *Curr Biol* **15**, 2199-2207 (2005).

60. Habedanck, R., Stierhof, Y.D., Wilkinson, C.J. & Nigg, E.A. The Polo kinase Plk4 functions in centriole duplication. *Nat Cell Biol* **7**, 1140-1146 (2005).
61. Godinho, S.A. *et al.* Oncogene-like induction of cellular invasion from centrosome amplification. *Nature* **510**, 167-171 (2014).
62. Guderian, G., Westendorf, J., Uldschmid, A. & Nigg, E.A. Plk4 trans-autophosphorylation regulates centriole number by controlling betaTrCP-mediated degradation. *J Cell Sci* **123**, 2163-2169 (2010).
63. Kosar, M. *et al.* Senescence-associated heterochromatin foci are dispensable for cellular senescence, occur in a cell type- and insult-dependent manner and follow expression of p16(ink4a). *Cell Cycle* **10**, 457-468 (2011).
64. Kang, C. *et al.* The DNA damage response induces inflammation and senescence by inhibiting autophagy of GATA4. *Science* **349**, aaa5612 (2015).
65. Rodier, F. *et al.* Persistent DNA damage signalling triggers senescence-associated inflammatory cytokine secretion. *Nat Cell Biol* **11**, 973-979 (2009).
66. Santaguida, S. *et al.* Chromosome Mis-segregation Generates Cell-Cycle-Arrested Cells with Complex Karyotypes that Are Eliminated by the Immune System. *Dev Cell* **41**, 638-651 e635 (2017).
67. Soto, M. *et al.* p53 Prohibits Propagation of Chromosome Segregation Errors that Produce Structural Aneuploidies. *Cell Rep* **19**, 2423-2431 (2017).

Figure 1

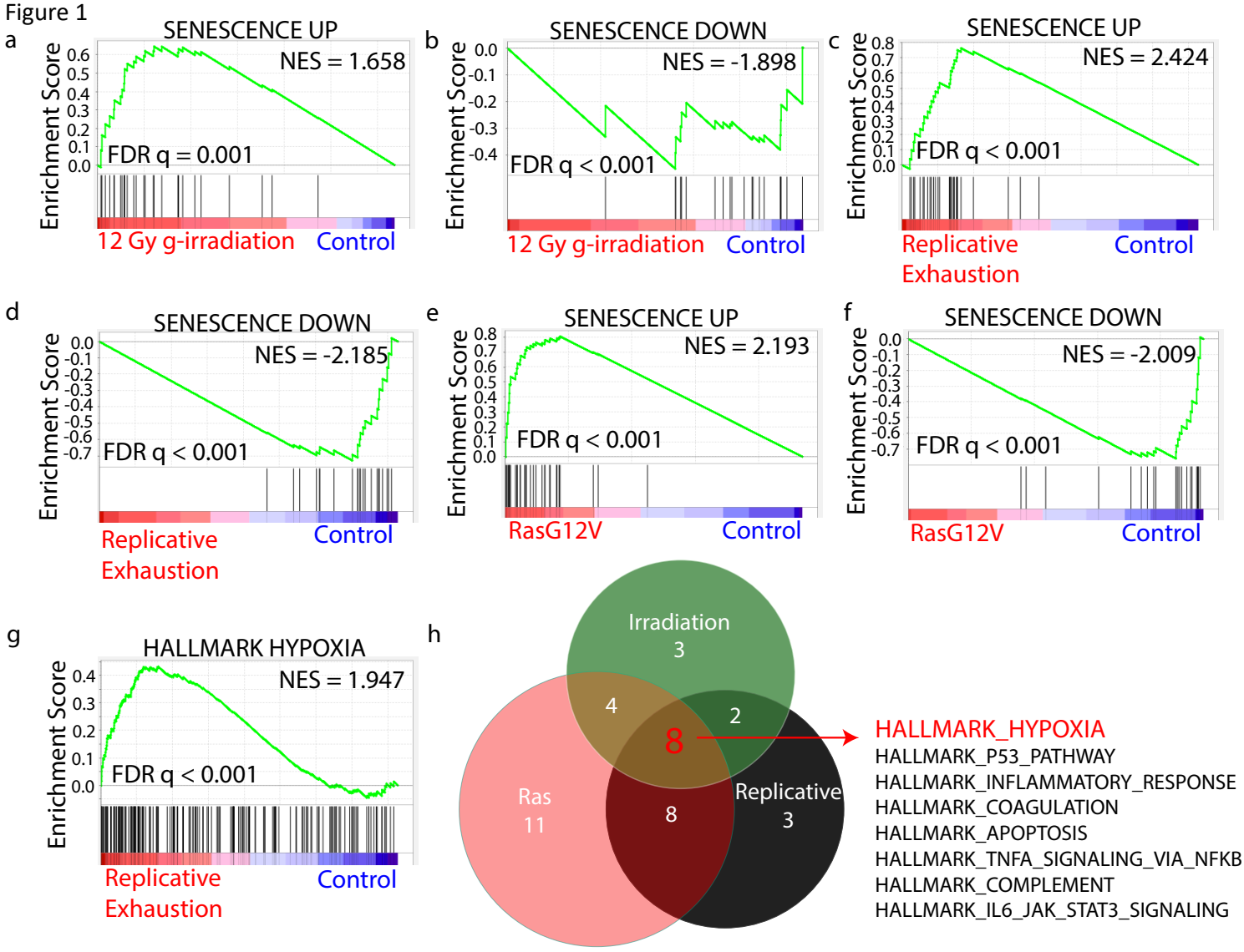

Common Hallmarks

Ras & Replicative Senescence	Ras & Irradiation Senescence	Replicative & Irradiation Senescence
HALLMARK_ADIPOGENESIS	HALLMARK_ALLOGRAFT_REJECTION	HALLMARK_KRAS_SIGNALING_DN
HALLMARK_CHOLESTEROL_HOMEOSTASIS	HALLMARK_ANGIOGENESIS	HALLMARK_MYOGENESIS
HALLMARK_ESTROGEN_RESPONSE_EARLY	HALLMARK_EPITHELIAL_MESENCHYMAL_TRANSITION	
HALLMARK_HEME_METABOLISM	HALLMARK_KRAS_SIGNALING_UP	
HALLMARK_IL2_STAT5_SIGNALING		
HALLMARK_INTERFERON_GAMMA_RESPONSE		
HALLMARK_PROTEIN_SECRETION		
HALLMARK_XENOBIOTIC_METABOLISM		

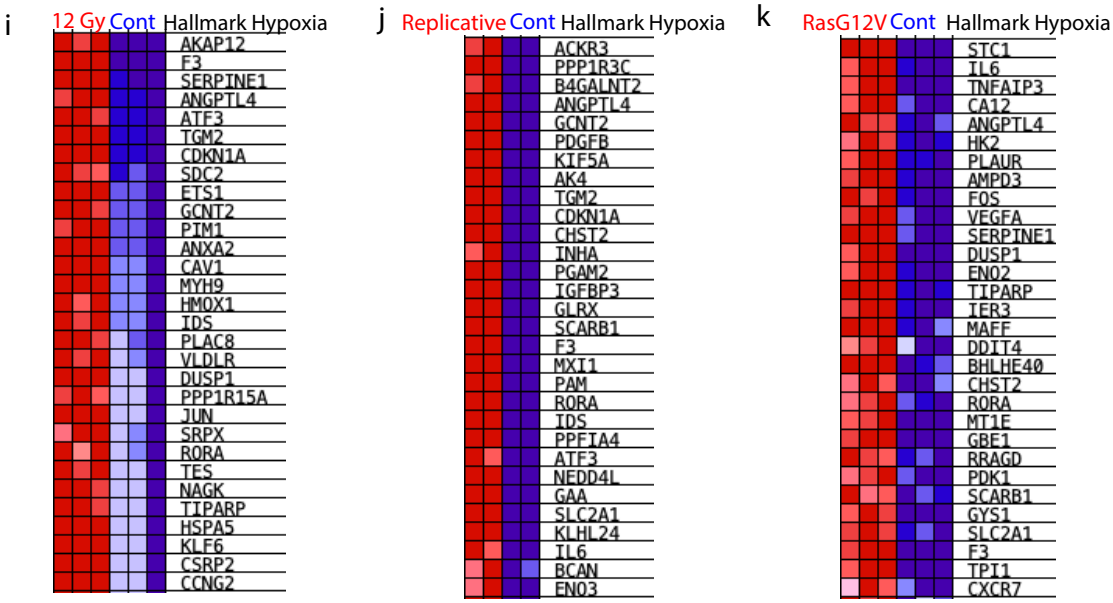

Figure 2

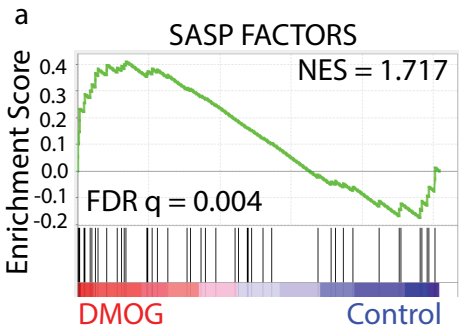
a
SASP FACTORS
NES = 1.717
FDR q = 0.004
Enrichment Score
0.4
0.3
0.2
0.1
0.0
-0.1
-0.2
DMOG
Control

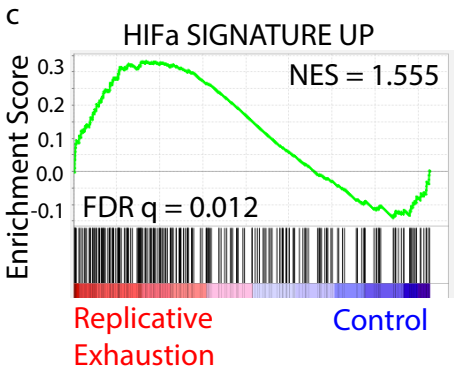
c
HIFa SIGNATURE UP
NES = 1.555
FDR q = 0.012
Enrichment Score
0.3
0.2
0.1
0.0
-0.1
Replicative
Exhaustion
Control

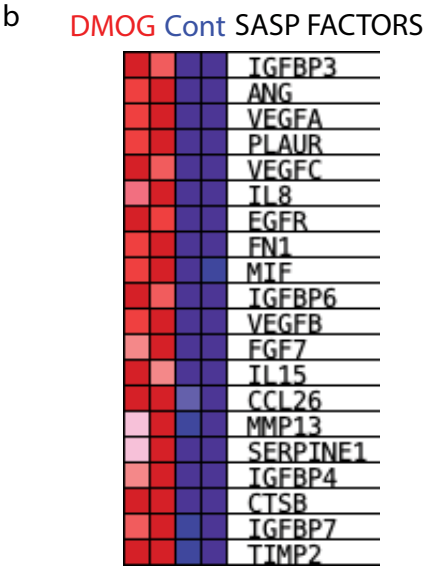
b
DMOG Cont SASP FACTORS
IGFBP3
ANG
VEGFA
PLAUR
VEGFC
IL8
EGFR
FN1
MIF
IGFBP6
VEGFB
FGF7
IL15
CCL26
MMP13
SERPINE1
IGFBP4
CTSB
IGFBP7
TIMP2

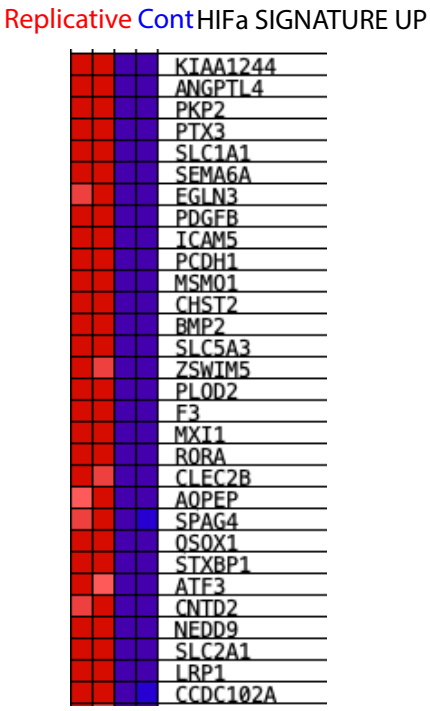
d
Replicative Cont HIFa SIGNATURE UP
KIAA1244
ANGPTL4
PKP2
PTX3
SLC1A1
SEMA6A
EGLN3
PDGFB
ICAM5
PCDH1
MSMO1
CHST2
BMP2
SLC5A3
ZSWIM5
PLOD2
F3
MXI1
RORA
CLEC2B
AOPEP
SPAG4
OSOX1
STXBP1
ATF3
CNTD2
NEDD9
SLC2A1
LRP1
CCDC102A

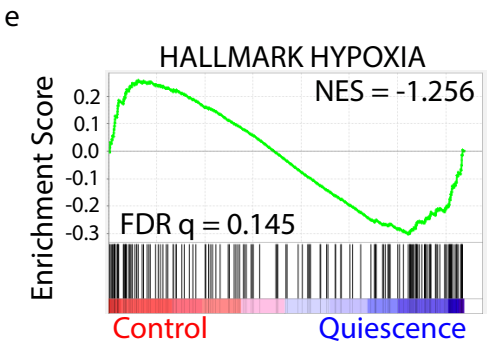
e
HALLMARK HYPOXIA
NES = -1.256
FDR q = 0.145
Enrichment Score
0.2
0.1
0.0
-0.1
-0.2
-0.3
Control
Quiescence

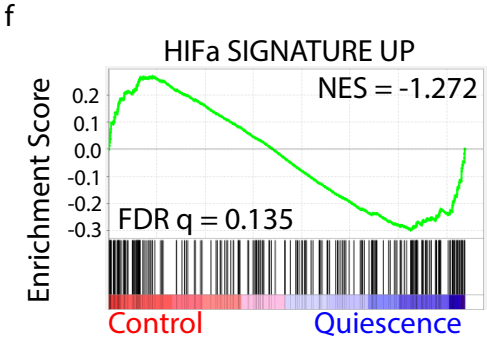
f
HIFa SIGNATURE UP
NES = -1.272
FDR q = 0.135
Enrichment Score
0.2
0.1
0.0
-0.1
-0.2
-0.3
Control
Quiescence

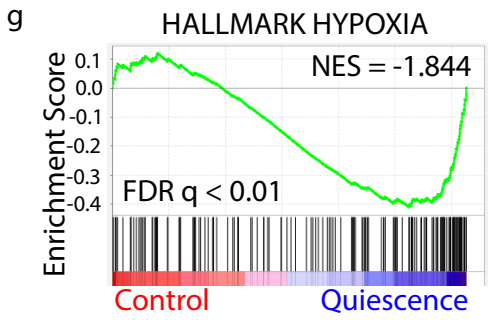
g
HALLMARK HYPOXIA
NES = -1.844
FDR q < 0.01
Enrichment Score
0.1
0.0
-0.1
-0.2
-0.3
-0.4
Control
Quiescence

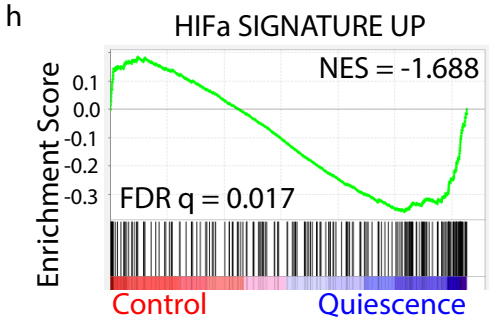
h
HIFa SIGNATURE UP
NES = -1.688
FDR q = 0.017
Enrichment Score
0.1
0.0
-0.1
-0.2
-0.3
Control
Quiescence

Figure 3

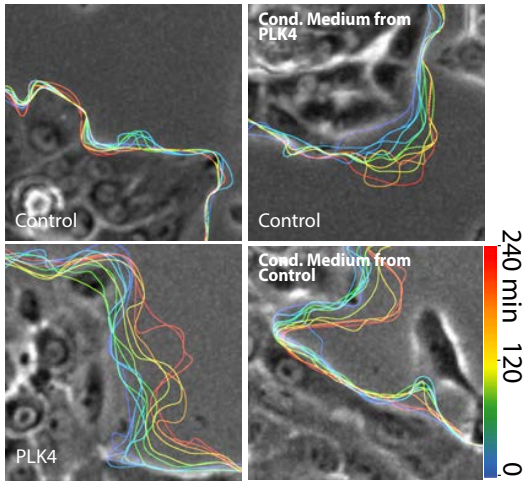
a
Control
Cond. Medium from PLK4
Control
PLK4
Cond. Medium from Control
240 min
120
0

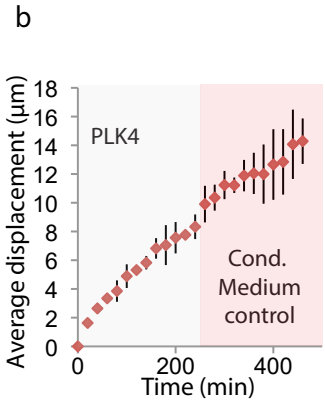
b
Average displacement (µm)
PLK4
Cond. Medium control
Time (min)

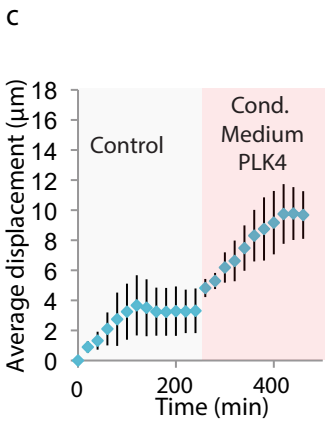
c
Average displacement (µm)
Control
Cond. Medium PLK4
Time (min)

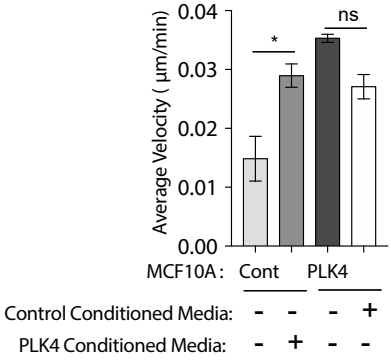
d
Average Velocity (µm/min)
ns
MCF10A : Cont PLK4
Control Conditioned Media: - - - +
PLK4 Conditioned Media: - + - -

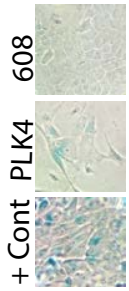
e
608
PLK4
+ Cont

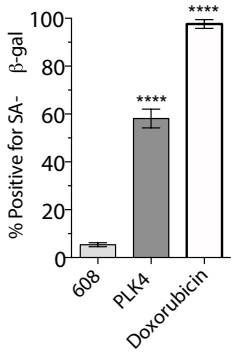
f
% Positive for SA- β-gal
608
PLK4
Doxorubicin

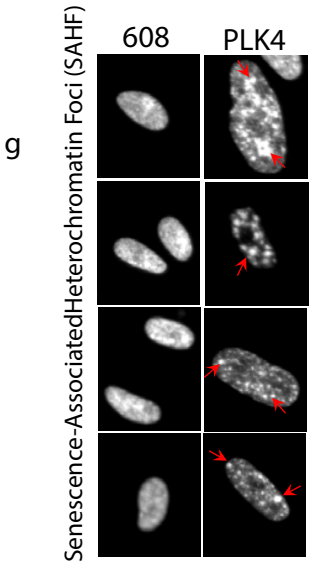
g
608
PLK4
Senescence-AssociatedHeterochromatin Foci (SAHF)

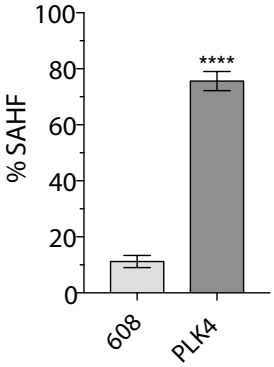
h
% SAHF
608
PLK4

Figure 4

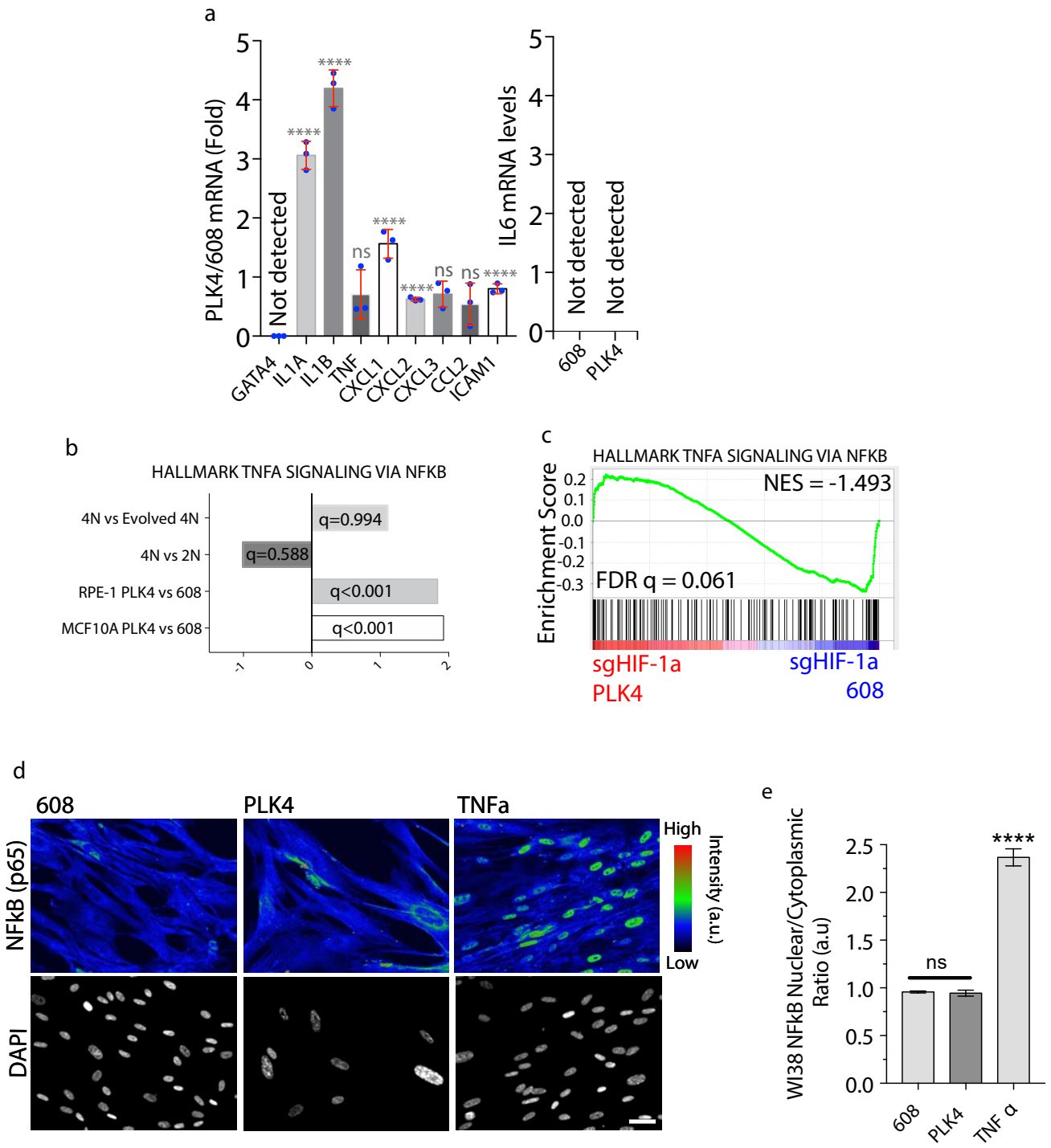
a
PLK4/608 mRNA (Fold)
Not detected
****
****
ns
****
****
ns
ns
****
GATA4
IL1A
IL1B
TNF
CXCL1
CXCL2
CXCL3
CCL2
ICAM1
IL6 mRNA levels
Not detected
Not detected
608
PLK4
b
HALLMARK TNFA SIGNALING VIA NFKB
4N vs Evolved 4N
4N vs 2N
RPE-1 PLK4 vs 608
MCF10A PLK4 vs 608
q=0.994
q=0.588
q<0.001
q<0.001
c
HALLMARK TNFA SIGNALING VIA NFKB
Enrichment Score
NES = -1.493
FDR q = 0.061
sgHIF-1a
PLK4
sgHIF-1a
608
d
608
PLK4
TNFa
NFkB (p65)
DAPI
High
Low
Intensity (a.u.)
e
WI38 NFkB Nuclear/Cytoplasmic Ratio (a.u)
ns
****
608
PLK4
TNF α

Figure 5

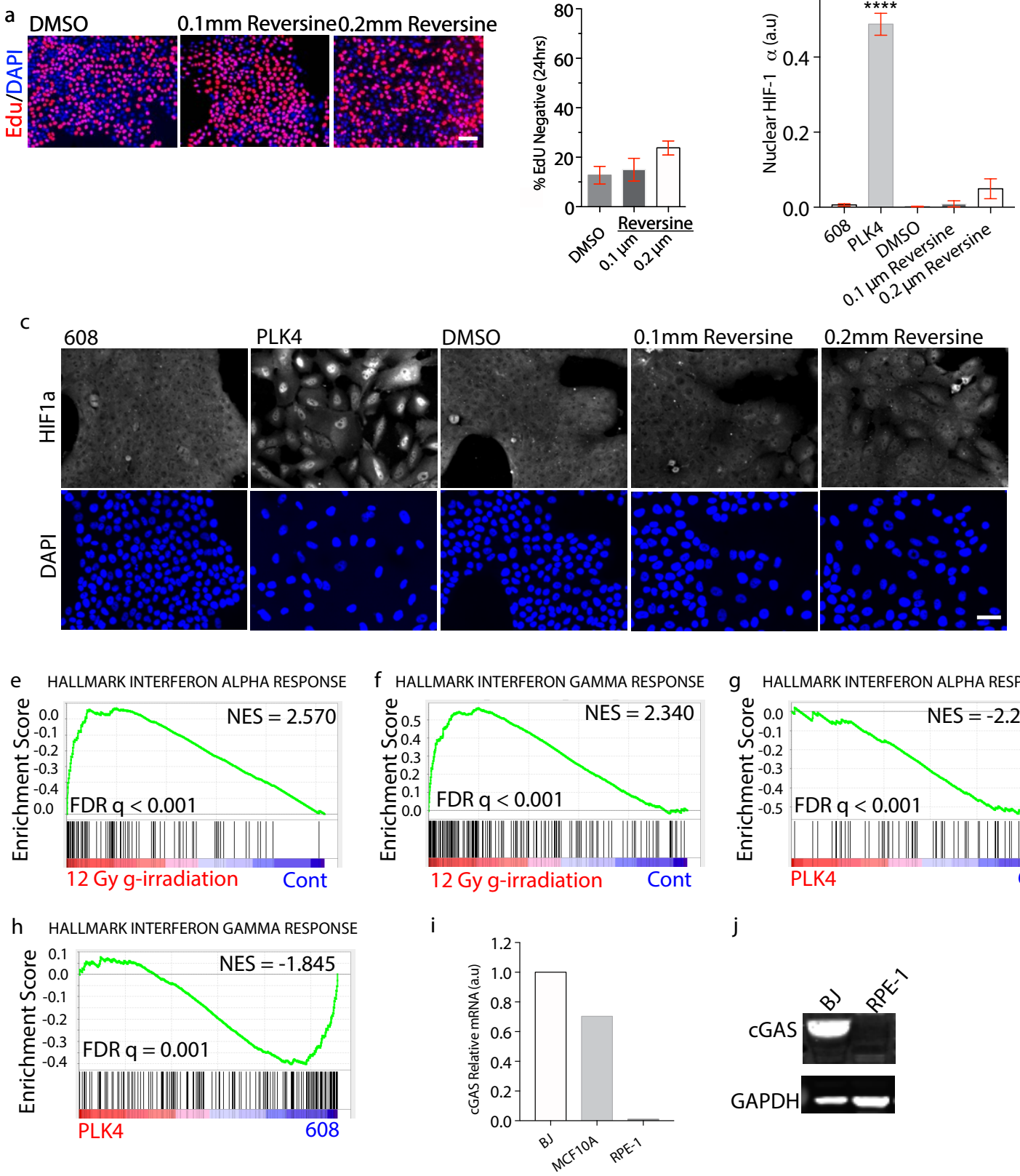
a
DMSO
0.1mm Reversine
0.2mm Reversine
Edu/DAPI
b
% EdU Negative (24hrs)
80
60
40
20
0
DMSO
Reversine
0.1 µm
0.2 µm
d
Nuclear HIF-1 α (a.u)
****
0.4
0.2
0.0
608
PLK4
DMSO
0.1 µm Reversine
0.2 µm Reversine
c
608
PLK4
DMSO
0.1mm Reversine
0.2mm Reversine
HIF1a
DAPI
e
HALLMARK INTERFERON ALPHA RESPONSE
Enrichment Score
NES = 2.570
FDR q < 0.001
12 Gy g-irradiation
Cont
f
HALLMARK INTERFERON GAMMA RESPONSE
Enrichment Score
NES = 2.340
FDR q < 0.001
12 Gy g-irradiation
Cont
g
HALLMARK INTERFERON ALPHA RESPONSE
Enrichment Score
NES = -2.259
FDR q < 0.001
PLK4
608
h
HALLMARK INTERFERON GAMMA RESPONSE
Enrichment Score
NES = -1.845
FDR q = 0.001
PLK4
608
i
cGAS Relative mRNA (a.u)
1.2
1.0
0.8
0.6
0.4
0.2
0.0
BJ
MCF10A
RPE-1
j
BJ
RPE-1
cGAS
GAPDH